



# Influence of short-range order on precipitate orientation relationships in aluminum containing FCC high entropy alloys

Elaf A. Anber<sup>a</sup>, Daniel L. Foley<sup>a</sup>, James L. Hart<sup>a,b</sup>, Howie Joress<sup>c</sup>, Brian DeCost<sup>c</sup>, Roger Doherty<sup>d</sup>, Peter K. Liaw<sup>e</sup>, Diana Farkas<sup>f</sup>, Anatoly I. Frenkel<sup>g,h,\*</sup>, Mitra L. Taheri<sup>a,\*\*</sup>

<sup>a</sup> Department of Materials Science & Engineering, Johns Hopkins University, Baltimore, MD, USA

<sup>b</sup> Department of Materials Science and Engineering, Cornell University, Ithaca, NY, USA

<sup>c</sup> Materials Measurement Science Division, National Institute of Standards and Technology, Gaithersburg, MD, USA

<sup>d</sup> Department of Materials Science and Engineering, Drexel University, Philadelphia, PA, USA

<sup>e</sup> Department of Materials Science and Engineering, University of Tennessee Knoxville, Knoxville, TN, USA

<sup>f</sup> Department of Materials Science and Engineering, Virginia Polytechnic Institute, Blacksburg, VA, USA

<sup>g</sup> Department of Materials Science and Chemical Engineering, Stony Brook University, Stony Brook, NY, USA

<sup>h</sup> Chemistry Division, Brookhaven National Laboratory, Upton, NY, USA

## ARTICLE INFO

### Keywords:

High entropy alloys  
Compositional complexity  
Orientation relationship  
Local chemical order

## ABSTRACT

High entropy alloy (HEA) phase evolution is governed by the competing roles of high configurational entropy and enthalpy of mixing, including severe lattice distortion, and local, or short range, atomic order. While HEAs have seen unprecedented interest over the last decade, many promising applications have not been realized due to limitations in secondary phase, or precipitate, control. Through high resolution microscopy and spectroscopy coupled with molecular dynamics simulations, we examine the role of chemical complexity on the evolution of precipitates, and specifically on their orientation relationships with their host matrices. Microstructural, chemical, and local order measurements are coupled with atomistic simulations of the structure and energy of the Face Center Cubic (FCC)/Body Center Cubic (BCC)B2 interface, in various possible orientations, using model interatomic potentials. Our local order measurements at the nanometer scale revealed that Cr-(Co/Ni/Fe) bonding becomes less favorable after aging. This finding aligns with our microstructural observations, which show lower Cr and Al content in the FCC phase post-aging. We experimentally observed a non-typical orientation relationship between B2-BCC and FCC matrices was stabilized, which we attribute to this chemical complexity. Our atomistic simulations reveal the significant effect of chemical complexity and local ordering on interface energies. Critically, we connect the local chemical order with the formation of high energy interfaces that lead to unusual orientation relationships. The relationship between local order and the orientation relationships landscape of precipitates within a microstructure presents an opportunity for tuning alloy properties at the level of atomic bonding.

## 1. Introduction

High entropy alloys (HEAs), also referred to as compositionally complex alloys (CCAs) or multiprincipal element alloys (MPEAs), have attracted much attention due to their novel mechanical and structural properties. The vast compositional space of HEAs and their resulting microstructures yields a wealth of opportunity for improved mechanical properties [1–7]. In addition to complex local order strengthening effects [8], precipitate strengthening has been demonstrated in HEAs [9].

For refractory HEAs (or RHEAs) combinations of precipitates have been explored [10,11], but there remains a lack of a systematic approach to predictively understand mechanisms for room-temperature ductility and high creep strength [12–20]. Although precipitate evolution provides a path to marry strength and ductility in HEAs by coherent precipitate strengthening [21] and dual phase stabilization [22], a solution that controls the formation and stability of these phases has not been realized. One way of stabilizing precipitates is through the control of orientation relationships (ORs) [23,24].

\* Corresponding author. Department of Materials Science and Chemical Engineering, Stony Brook University, Stony Brook, NY, USA.

\*\* Corresponding author. Department of Materials Science & Engineering, Johns Hopkins University, Baltimore, MD, USA.

E-mail addresses: [anatoly.frenkel@stonybrook.edu](mailto:anatoly.frenkel@stonybrook.edu) (A.I. Frenkel), [mtaheri4@jhu.edu](mailto:mtaheri4@jhu.edu) (M.L. Taheri).

Crystallographic ORs, which describe the atomic fit between a nucleating precipitate and its parent phase [25,26], play an important factor in controlling the mechanical properties of metals and alloys, dictating dislocation glide pathways [27]. Understanding ORs is critical for realizing coherent interfaces between matrix and precipitates in HEAs. An OR is specified crystallographically by a pair of planes and directions, as in  $\frac{1}{A}/\frac{1}{B}$ , with  $\langle uvw \rangle_A // \langle uvw \rangle_B$ , as OR formation depends strongly on the lattice parameter mismatch of the crystals involved [27]. Between a BCC crystal and an FCC crystal, there are five common ORs reported: Bain, Kurdjumov and Sachs (K-S), Nishiyama and Wasserman (N-W), Greninger and Troiano (G-T), and Pitsch [28]. Newly distinct ORs, however, have been reported between BCC and FCC systems in an austenitic stainless steel [29]. He et al. [29] presented new ORs between austenite ( $\gamma$ -FCC) and martensite ( $\alpha'$ -BCC), formed by the relative rotation of  $-12.8^\circ$  from the Pitsch, in which [110] FCC//[111] BCC. Another new OR between delta-ferrite and austenite was observed in solidification microstructures of 304L and 309S austenitic stainless steels and a ternary Fe-Cr-Ni alloy [30]. This new OR (111) BCC//(110) BCC and [110] FCC//[110] BCC, had not been previously reported for BCC-FCC systems [30]. In a recent study of HEAs [31], three typical ORs for the B2 phase in  $Al_{0.3}CoCrFeNi$  were found within the same microstructure: KS, NW, and Pitsch. In another study of a similar HEA with a slight increase in Al, Rao et al. [32], reported *two new ORs* for the NiAl-B2 phase in  $Al_{0.5}CoCrFeNi$  and  $Al_{0.7}CoCrFeNi$  at room temperature, in which [001]BCC//[001]FCC and [011] B2//[11 $\sqrt{2}$ ] FCC. While these results marked a step forward in gathering additional information about the precipitation behavior in HEAs, and in particular  $Al_xCoCrFeNi$ , the mechanistic landscape of OR formation for BCC phases in the same alloy system is unclear. Alloy complexity, such as that exhibited by steels in the above-mentioned cases, seemed to dictate the multiplicity of ORs, however only the HEAs exhibited new, unique ORs. The presence of multiple, unique ORs suggests a dependency on local chemistry of a given alloy but exactly what underlies this OR-chemistry relationship isn't entirely understood.

Local chemical order (LCO) describes the preference in local chemistry of elements within a lattice that arises due to negative enthalpy of mixing believed to be more pronounced in HEAs [33–40]. Li et al. [41] studied the LCO in NiCoCr alloys at temperature between 649 K and 1349 K (376 °C and 1076 °C) using atomistic simulations. The study suggested that the CoCrNi alloy develops local Ni segregation and Co-Cr ordering with decreasing annealing temperature. Another study on CoCrNi by Foley, Barnett et al. [42] found similar localized segregation of Ni away from CoCr, which in turn resulted in nanoscale domains of broken FCC symmetry, similar to strain glass alloys. Maiti et al. [43], revealed the presence of short-range clustering in TaNbHfZrTi refractory HEAs after annealing at 2073 K (1800 °C) for 24 h, which led to a notable yield strength of 2310 MPa. Even in conventional alloys, local chemical segregation can help stabilize the formation of secondary phases by varying the interfacial energy for precipitation [44]. Compositional fluctuations/ordering in complex alloys can lead to local segregation, and their chemical complexity can result in unusual ORs in two-phase materials. Specifically, chemical fluctuation/ordering alters the interfacial energy landscape, enabling the formation of high-energy interfaces. It also induces a change in lattice parameter (lattice distortion), and as a result, the formation of uncommon ORs [45]. Feng et al. [46], for example, reported that ORs and morphology of the precipitates in magnesium alloys were varied with the concentration of Sn in the solid solution. Understanding the degree of LCO in HEAs will provide a step forward in stabilizing precipitates at high temperature via tuning their ORs.

This paper elucidates the relationship between ORs and the complex chemical and energetic landscape in HEAs using a coupled multiscale microscopy and simulation approach. We examined the relationship between chemical complexity and the ORs of the BCC structure phases in the  $Al_{0.3}CoCrFeNi$  high entropy alloys using compositional and structural analyses via transmission electron microscopy TEM(TEM). To

better understand the formation mechanisms of multiple different ORs that can arise in complex alloys, we perform atomistic simulation studies of the structure and energy of the FCC/B2 interface, in various possible orientations, using molecular dynamics calculations [46].

The results lead to a mechanistic foundation for stabilizing multi-phase HEAs at high temperatures which provides a piece of new knowledge for predictive alloy development. The multiplicity of ORs, including unique and new ORs, found in HEAs is a function of the chemical and energetic complexities associated with these alloy systems. Specifically, the local energetic fluctuations driven by compositional complexity give rise to a possible multiplicity of ORs in a microstructure by enabling local energetic minima via variations in coordination chemistry, allowing for ORs that in a single-component system would exhibit higher theoretical interfacial energies. Additionally, lattice distortion, dictated by LCO, can play a significant role in the various nucleation and growth mechanisms responsible for OR formation.

## 2. Methods

### 2.1. Alloy preparation and microstructure evolution characterization

Ingots of  $Al_{0.3}CoCrFeNi$  were produced by vacuum-induction melting followed by hot isostatic pressing at (1477 K) 1204 °C and 103 MPa for 4 h. To ensure chemical homogeneity, the alloys were subsequently heat treated at 1523 K (1250 °C) for 2 h. As-homogenized ingots were sliced into 300  $\mu$ m thick samples by electrical discharge machining, followed by conventional metallographic preparation for TEM [47]. In our previous work on the  $Al_xCoCrFeNi$  system [48–51], we designed a study concentrating on the acceleration of the precipitation kinetics in  $Al_{0.3}CoCrFeNi$  via *in-situ* and *ex-situ* TEM heating techniques, we observed the formation of secondary phases using a high density of surface nucleation sites in the thin foil at a temperature between 823 K and 1173 K (550 °C and 900 °C). Our studies revealed the formation of an additional intermediate phase, where hundreds of hours of annealing time are predicted for this phase to be observed during *ex-situ* experiments. To verify the ORs between the BCC and FCC phases, in this study, we selected 973 K (700 °C), 500 h *ex-situ* heated alloy. We observed B2 precipitates in the aged condition formed during the *ex-situ* annealing processes. Here, we compare the ORs between the BCC-B2 phase and the FCC matrix. To confirm the ORs between the two phases, we tilted the specimen so that the interface between the primary and secondary phases was approximately edge-on with respect to the optical axis of the microscope. This was done by tilting to minimize the apparent “width” of the boundary. We then relied on both selected area electron diffraction and the Fourier transforms of high-resolution TEM images to crystallographically determine the OR. The out of plane direction was determined by indexing the Bragg pattern of each phase and the boundary plane was determined by determining which direction was running perpendicular to the edge-on interface.

To characterize local order, we used Extended X-ray Absorption Fine Structure (EXAFS) to study the nearest neighboring bond distribution in the as-homogenized alloy averaged over the length scale comparable to the sample dimensions and extended electron energy loss fine structure (EXELFS) [52–54] to study this distribution in nanometer-scale regions near precipitates in the aged alloy, relevant to OR formation. While techniques such as synchrotron EXAFS also provide sensitivity to local bonding distributions in bulk and nanoscale alloys in the millimeter to micrometer range of the X-ray beam spot sizes [55–62], EXELFS offers nanometer spatial resolution, which facilitates localized measurements changes of fine-scale diffusional processes. Local analysis through EXELFS can reveal spatial fluctuations in order relevant to energy minima and localized changes in ORs. In contrast, relying solely on bulk or EXAFS analysis would fail to extract such details. Details regarding EXAFS and EXELFS analysis are available in the online supplementary information. In this study, we applied EXAFS to measure the global LCO in a homogenized alloy and then utilized EXELFS to assess LCO locally

within the FCC phase after aging. The same relationships between the coordination numbers and bond lengths of different atomic pairs in the alloys used in EXAFS to determine the details of mixing, segregation, and short-range order were applied to the analysis of EXELFS data.

## 2.2. OR simulation

To test our overarching hypothesis that order and the resulting structural, chemical, and energetic variations, controls OR formation, the alloy system of FeNiCrCoAl, was chosen as a model system for its ordering tendency and its ability to form predictable precipitates. In this model system, the binaries with Al have significantly negative heats of mixing and therefore, a strong tendency for ordering. Embedded atom model (EAM) interatomic potentials have been developed recently to represent idealized FCC mixtures of Fe–Ni–Cr–Co–Al at near-equiatomic compositions [46,63]. In these potentials, mixed pair interactions involving Al were developed using a mix of the component pair functions fitted to known intermetallic properties. The binary mixtures in the model system containing Al yield significant ordering and reproduce the relatively large atomic size difference between Al and the other components.

Molecular dynamics simulations were performed to investigate the possible contributing factors to novel ORs, including short-range order (SRO) (both chemical and structural), dislocation behavior and distribution, and any elastic strain contributions. The prediction of local order at precipitate/matrix interfaces was complemented by experimental observations to understand the effects that these fluctuations have on the precipitate evolution and OR multiplicity. The interatomic potentials used here have been developed to represent highly idealized FCC mixtures of Fe–Ni–Cr–Co–Al at near equiatomic compositions [46]. The potential was developed to predict heats of mixing of all binary equiatomic random FCC mixtures not containing Al as low, but significant ordering appears in alloys containing Al, driven by a large atomic size difference. The potentials can predict the relative stability of FCC quinary mixtures, as well as ordered L12 and B2 phases as a function of Al content. These predictions are in qualitative agreement with the findings of microstructural experiments observed via TEM, as will be shown in the results section. This interatomic potential set is developed to resemble, but not model precisely, the properties of this complex system, aiming at providing a tool to explore the consequences of the addition of a large size-misfit component into a high entropy mixture that develop multiphase microstructures. It is used here to understand basic trends in the nature of the interface between the FCC and B2 phases in an Al containing complex alloy.

The LAMMPS molecular dynamics code [64], along with the OVITO simulation package [63] were used to perform the simulations herein. Digital samples included a cubic B2 precipitate with 7.2 nm edge length embedded in an FCC matrix approximately twice the size of the precipitate. The interface structure was relaxed at constant zero pressure in all directions and equilibrated at 300 K for 100 ps. The matrix phase is a random equiatomic FCC CrFeCoNi alloy, and the B2 phase was 50 % Al with the remaining four elements distributed at random in equiatomic proportion. The compositions of the bulk phases are given in Table 3. The interatomic potentials have been developed to predict these two phases at 300 K, with potential cohesive energies per atom of  $-4.363$  eV for the FCC matrix and  $-3.962$  eV for the B2 phase. Three ORs were studied: the KS, the Bain, and a non-typical OR identified in the present experiments, which is an example of a non-conventional ORs that can occur in complex HEAs.

In the analysis of the resulting structures, the atoms in the relaxed sample were assigned to the FCC matrix, the B2 precipitate, or the interface using the common neighbor analysis algorithm (part of the OVITO package [65]). The average potential energy of atoms in the interface was obtained and served as a basis for the estimation of the interface energy.

The interface energies were estimated from the difference of this

average energy of atoms in the interface to the average of the FCC and B2 phase cohesive energies per atom ( $-4.1625$  eV), the number of atoms in the interface, and the corresponding interface areas (cube faces of  $51.84$  nm<sup>2</sup> each). For each of the three ORs studied, this procedure was performed separately for the three different interface plane orientations of the interface present in the cuboid precipitate. This yielded estimates of the average interface energy for each OR, as well as the variability of this energy in each case. The simulations also allowed the study of the composition of the relaxed interface in each case that resulted from the relaxation process. The estimates of interface energy values were used in a classical nucleation theory model to assess the effects of interface energy variation on nucleation barriers.

## 3. Results and discussion

Using a combination of theory and multiscale microscopy, the degree of chemical complexity was correlated with the nucleation and growth habits of precipitates in HEAs, and specifically how this chemical and structural landscape gives rise to OR multiplicity. As described above, these studies include not only the characterization of local order and unique ORs in these alloys but also seek to link these two phenomena through calculations of lattice and interfacial energies, measurements of interfacial elastic and plastic strains, and evaluation of the dislocation-based processes that precede and facilitate precipitate formation.

### 3.1. Local chemical order

The microstructure of as-homogenized and aged Al<sub>0.3</sub>CoCrFeNi has been previously investigated [47–50], where the as-homogenized alloy presents a single FCC phase and the aged (973 K (700 °C), 500 h) alloy consists of three phases: FCC-matrix, NiAl- B2, and Cr-BCC (Fig. 1A, and Supplementary Fig. 1). The NiAl- B2 and Cr-BCC phases consumed the Cr, Ni, and Al content of the FCC phase. As we showed in our previous work [48], the Cr and Al atomic concentrations decreased from 24 % to 7.4 %–8.7 % and 3.19 %, respectively, after aging due to the formation of NiAl- B2 and Cr-BCC phases. Cr and Al have the largest atomic radii [1,66] compared to Fe, Ni, and Co. Therefore, smaller atomic size differences and lower lattice distortion are expected in the FCC phase of the aged alloy. The microstructural analysis was complemented by EXAFS and EXELFS analyses to examine the local bonding environment of each species. Because synchrotron EXAFS averages over a large sample area (of the order of one square millimeter) and because of the difficulty of excluding the matrix from the precipitates formed during aging, here, we rely on spatially resolved EXELFS [52], to examine the chemical order in the FCC-matrix after aging (Fig. 1). Fig. 1 shows a comparison of EXAFS Fourier transform magnitude (in r-space) for Cr (Fig. 1B), Co (Fig. 1C), and Ni (Fig. 1D) absorbers in as-homogenized and aged alloys. Due to the similarity of the photoelectron scattering amplitudes and phases of Co/Cr/Ni/Fe [60,67], we cannot quantify the contributions to EXAFS by the unique scattering pairs (e.g., Cr-Co, Cr-Cr, Cr-Ni and Cr-Fe) for the as-homogenized and aged data. Instead, we rely on the more crude but stable model that approximates all nearest neighbors to the absorber by a single atomic type and examines the difference in the best fit values of the length of such an effective “bond” for the as-homogenized and the aged alloys. The data in Fig. 1B–D shows that the first shell peaks around Cr, Co and Ni differ between the as-homogenized and the aged alloys. Quantitative analysis has been attempted using a simplified local structural model where Cr and Al scattering has been excluded from the fitting of Co/Cr/Ni and Fe absorber edges (details regarding EXAFS and EXELFS analysis are available in the online supplementary information and Supplementary Fig. 2–5). Based on this model, the average effective bond lengths (Supplementary Table 1) of Cr-M, Ni-M, and Co-M bonds decreased after aging. Cr and Al, which possess the largest atomic sizes in the alloy, also exhibit reduced concentrations within the matrix after aging, as confirmed by our Scanning Transmission Electron Microscopy

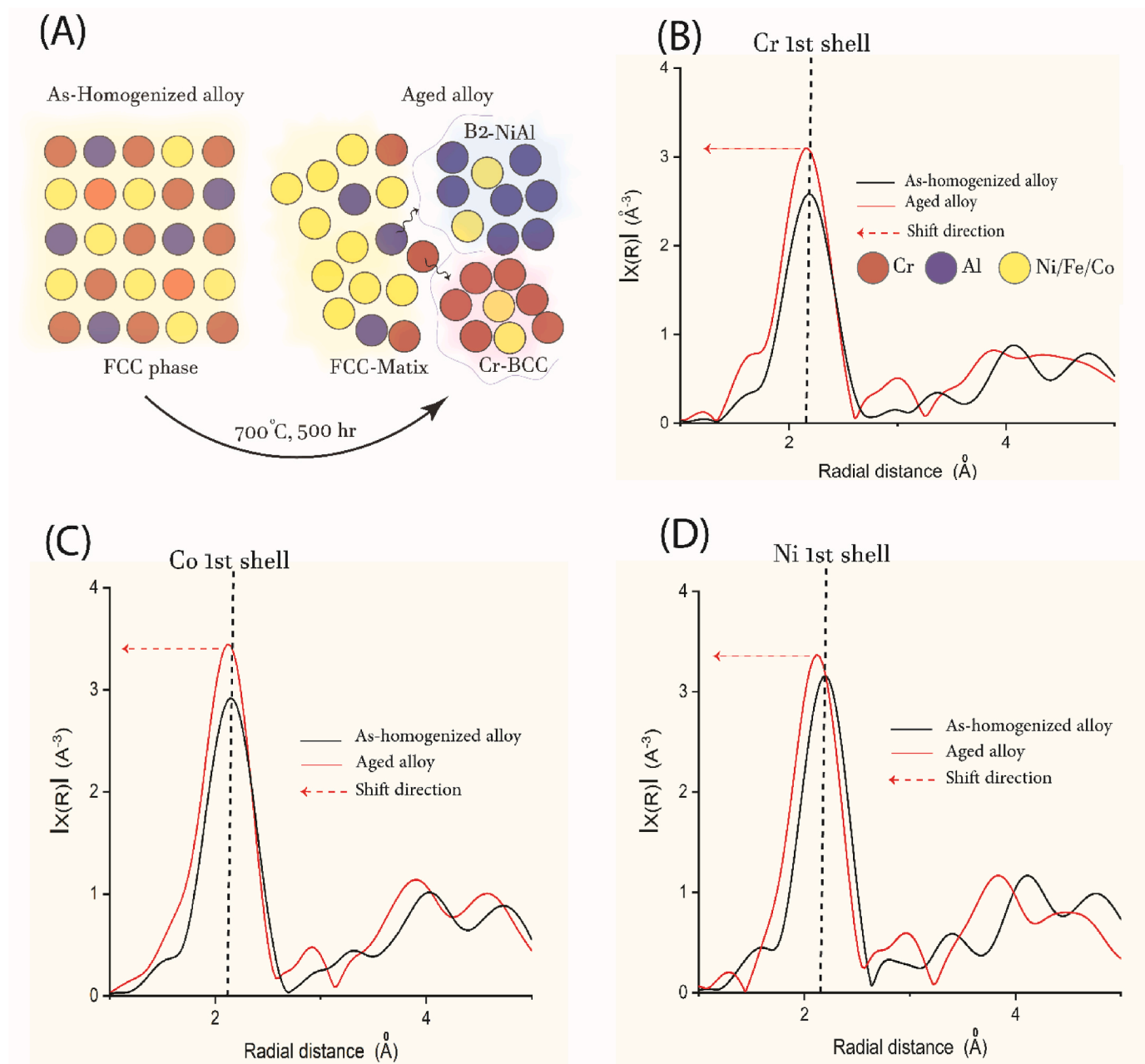


**Fig. 1.** Schematic representation of the microstructure of as-homogenized and aged alloys(A). Comparison of the R-space Cr(B), Co(c), and Ni(D) - K edge spectra for the as-homogenized alloy, as measured with EXAFS, compared to the aged alloy, as measured with EXELFS. The position of the peak associated with the first nearest neighbor shell shifts, indicating a change in bonding conditions. The absence of R-space data for Al is due to the challenges of obtaining reliable EXAFS signals at the low-energy Al K-edge, combined with limitations in beamline capability for measurements at this energy.

(STEM)/Energy Dispersive X-ray Spectroscopy (EDS) [48] analysis. This compositional change is consistent with the reduction in bond length observed in the EXELFS data, suggesting that Cr–M bonding becomes less favorable after aging.

Changes in local chemical order have been linked to fluctuations in lattice energetics. One example of such a phenomenon is the changes in stacking fault energies in 3d-transition metal-based alloys such as CoCrFeMnNi and CoCrNi. Both DFT and MD simulations predict changes in the energetic cost of the formation of a stacking fault in the FCC lattice as a function of the specific chemical configuration of the atomic planes involved in fault formation [68–70]. Nonconstant stacking fault energies have been verified experimentally [71]. While these and other studies [72] have correlated these findings with mechanical response due to the critical role the stacking fault energy plays in the type of dislocations

that are available for plastic deformation, they also inform the present work since the stacking fault energy is essentially an interfacial energy like a phase boundary between a matrix and precipitate.

### 3.2. OR experimental determination

To verify the ORs between B2 and FCC phases, we utilized both selected area electron diffraction and the Fourier transforms of high-resolution TEM images. Fig. 2 contains TEM images of the BCC phases in an annealed  $\text{Al}_{0.3}\text{CoCrFeNi}$  HEAs and reveals unexpected ORs between BCC and FCC phases. Diffraction patterns from aged alloy show the common KS OR for the grain boundary (GB)- B2 phase (Fig. 2A). The rod-shaped B2 phase within the same sample, however, exhibits unusual ORs with the FCC matrix, where  $\langle 110 \rangle_{\text{FCC}} // \langle 100 \rangle_{\text{BCC}}$ , Fig. 2B-C.

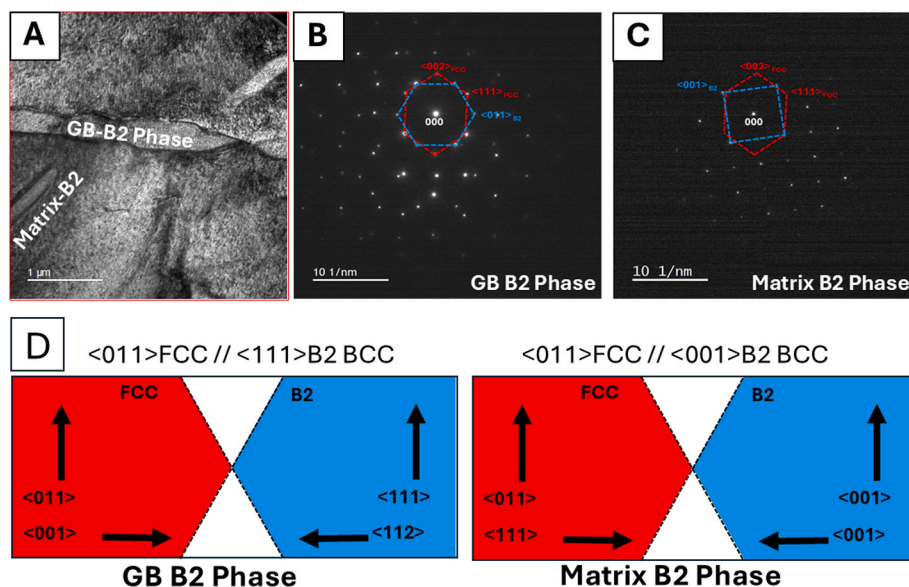


**Fig. 2.** The crystallographic ORs between BCC and FCC after heating at 700 °C for 500 h. TEM image of annealed alloy (A) and the corresponding SADPs from the B2 phase and the matrix shows the reflection of  $\langle 011 \rangle_{\text{FCC}}$  from the matrix and  $\langle 111 \rangle_{\text{BCC}}$  from GB-B2 phase, and  $\langle 001 \rangle_{\text{B2}}$  reflection from the matrix-B2 phase, (B, and C, respectively). A schematic diagram illustrates the orientational relationships between the B2 and FCC phases, showing the related directions based on the indexed zone axes (D). The results reveal an unusual OR between the FCC and matrix B2 phases.

The non-typical ORs can be attributed to the complex local chemistry observed in the as-homogenized and aged alloys, and the resulting energetic and structural fluctuations, in HEAs [69–73]. The chemical complexity (combined with SRO) can influence interfacial structure by modifying local bonding environments and energetics. These factors may contribute to the formation of non-typical orientation relationships by promoting specific atomic configurations that deviate from ideal lattice matching criteria. In other words, we believe that this formation of non-typical ORs can be attributed to the complex local chemistry in  $\text{Al}_x\text{CoCrFeNi}$  alloy system, a conjecture that has been made previously by the global HEA community [74]. For example, studies on the energetics of the  $\text{AlCoCrFeNi}$  system of HEAs have shown that due to the varying atomic radii and subsequent lattice distortion, the base lattice energy of the alloy can increase with increased complexity [75]. The increased lattice energy leads to a decreased barrier for nucleation of dislocations during deformation, while at the same time the distortion hampers dislocation kinetics due to fluctuations in the Peierls barrier [75]. The “rugged” energetic landscape of HEAs contrasts with conventional alloys that have relatively uniform lattice energies. Furthermore, these variable energetic environments give rise to nonuniform values of stacking fault energies [69,71,73–75], which in turn lead to anomalous dislocation behavior where sometimes partial and sometimes full dislocations are favored. Not only can these effects of complex chemical energetics affect dislocation processes (which itself affects precipitates formation in terms of providing nucleation sites and affecting kinetics), but it stands to reason that they could affect the nucleation and growth of precipitates (the stacking fault energy is, after all, essentially an interfacial energy). In fact, studies on Ni-Al and Ni-Fe alloys show significant differences in stacking fault energy between the ordered and disordered phases [76], directly highlighting the role atomic arrangement can play in modulating interfacial energetics. In fact, in Ni-based super alloys stacking faults themselves can provide nucleation sites for secondary phase formation, and the chemical ordering on those stacking faults can determine the precipitation type [77]. Controlling the degree of order in these alloys means tuning of the energetic landscape in the matrix, in turn allowing for the encouragement or suppression of more exotic microstructures than found in conventional alloys. This can not only affect the precipitation process of secondary phases itself, but the subsequent mechanical response as a result of that

process. Studies have shown that a careful balance of  $\kappa$  and B2 precipitation in  $\text{AlCoFeMnNi}$  alloys can lead to simultaneously high levels of strength in ductility due to the onset of slip band-refinement induced plasticity combined with precipitation and dispersion hardening [78]. The opportunity to tune alloy compositions and their local chemical order to stabilize unique combinations of microstructural features not achievable in conventional alloys.

### 3.3. OR simulation

This compositional complexity affects interface energies in various orientations. To illustrate these effects, Fig. 3 shows examples of different possible structures simulated in various orientation relationships, as well as average atomic cohesive energies as a function of the distance to the interface. Bins of 0.2 nm parallel to the interface were used for these averages. These results show a specific increase in energy in the interface region, that can be used to estimate the interface energy. These results also indicate that the interface has a certain thickness, resulting from the relaxation which we could estimate for each different interface orientation parameter. We observed wide variation in the structure and energetics of the interface simulated. We first estimated the interface thickness, using the number of atoms in the interface as obtained from the common neighbor analysis. Interface atoms were those that the analysis did not identify as belonging either to the matrix (FCC) or the precipitate (BCC). We estimate the interface thickness by dividing the sum of the atomic volumes of all atoms in the interface by the known interface area; we use atomic volumes estimated from the perfect lattice. Our estimates of the interface thicknesses ranged between 0.3 nm and 0.5 nm, depending on the orientation relationship and orientation of the interface plane. Estimates of the interface energy varied between 0.8  $\text{J}/\text{m}^2$  and 2  $\text{J}/\text{m}^2$ , depending on the orientation relationship and orientation of the interface plane. Table 1 reports the lowest values found for each OR, as well as the averages and the standard deviations over the 6 precipitate faces.

We also analyzed the composition of the interface atoms, again as obtained from the common neighbor analysis. The results presented in Table 2 reveal that the interface exhibits a relatively higher atomic concentration of Al, reaching up to 32 % Al, compared to the anticipated average composition of the matrix and precipitate, which is 25 % Al. We

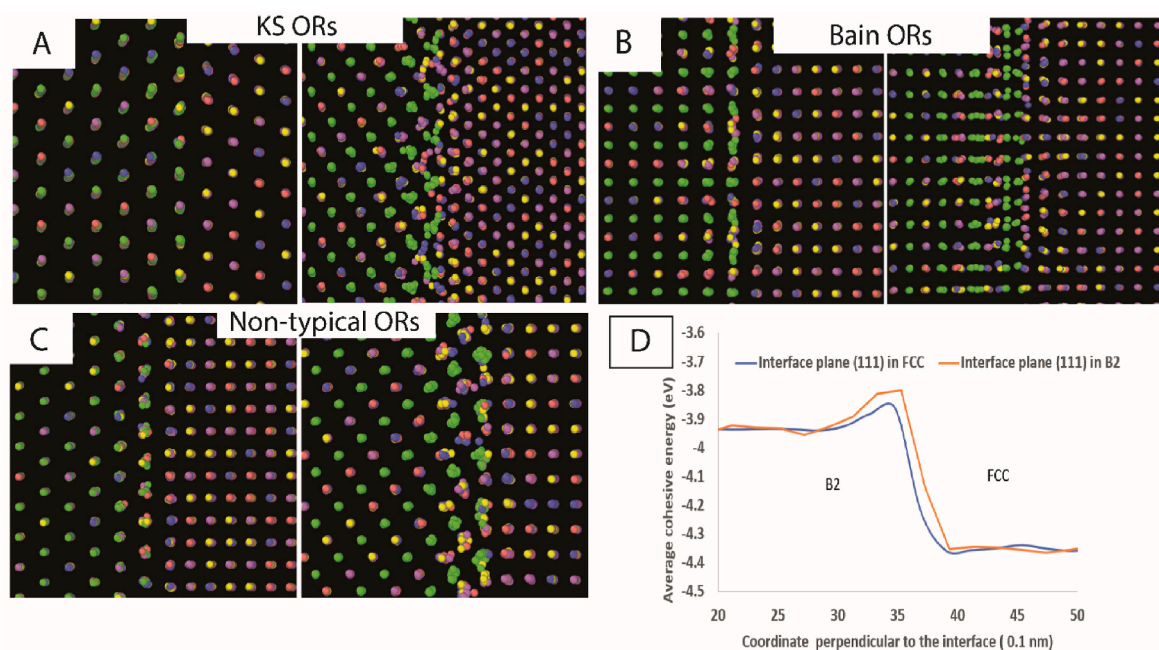


**Fig. 3.** Examples of possible interfacial structures simulated with various orientation relationships. (A, B) Structures based on the KS and Bain orientation relationships, respectively, which are commonly observed in FCC–B2 systems. (C) A non-typical orientation relationship constructed using the {100} plane of the B2 phase, based on the experimentally observed interface shown in Fig. 2. In all models, Al atoms are shown in green, with the B2 phase on the left and the FCC matrix on the right. (D) Average cohesive energy as a function of distance from the interface, calculated for the KS orientation relationship using two different interface plane orientations. Energy values are averaged over layers 0.2 nm thick. The KS and Bain models were selected as they are common orientation relationships between FCC and BCC phases. (For interpretation of the references to colour in this figure legend, the reader is referred to the Web version of this article.)

**Table 1**

Interface energies (J/m<sup>2</sup>) calculated for the interface of various orientations. Uncertainties indicate the standard deviation over the six precipitate faces.

	Lowest	Average
KS	0.74	1.17 ± 0.36
Bain	0.8	0.85 ± 0.07
Non-typical	1.37	1.79 ± 0.37

**Table 2**

Compositions of the phases and relaxed interfaces in the simulations (at. %).

Phases	Al	Co	Cr	Fe	Ni
FCC	0	25	25	25	25
B2	50	12.5	12.5	12.5	12.5
Inter KS	33	18	17	16	16
Inter Bain	28	18	18	18	18
Inter non-typical	32	17	17	17	16

note that this enrichment is due simply to the local relaxation of the interface since the time scale of our molecular dynamics simulations is too short to realize possible energy-driven segregation effects. Table 3

There was also some variability in the interface compositions depending on the OR, with interface compositions between 28 % and 32 % Al on an atomic basis. The simulation results also showed a variety of

**Table 3**

Ordering effects on cohesive energy and stacking fault energy as a function of Al content in the FCC phase predicted by the EAM potentials.

Al content (at %)	Cohesive energy (kJ/mol)	Stacking fault energy (mJ/m <sup>2</sup> )
0	0	0
5	−0.4	−5
10	−1.1	−25
15	−2.2	−26

different possible interface structures. Fig. 4 shows some examples of this variability, for each of the three OR simulated. These structures show different degrees of atomic matching at the interface, as exemplified in Fig. 3.

Besides the interface energy and structure, we monitored the presence of interface dislocations and dislocations emitted into the FCC matrix. This was done using the DXA dislocation extraction algorithm in OVITO package [65]. The KS OR sample showed Shockley partial dislocations emitted into the matrix from the interface. The Bain OR structure showed a network of 1/6[110] stair-rod dislocations as part of the interface, these are shown in Fig. 4. The unusual OR exhibited no misfit dislocations.

These results are for a model system with no Al in the matrix and the B2 precipitate with perfect order with an Al atomic concentration of 50 %. The observed variability in interface energies is expected to be even more important if the degree of order in the matrix or in the precipitates also varies. As an example of these effects, we computed the effects of ordering in the matrix by comparing alloys with random distributions of Al (disordered) with those where no Al–Al nearest neighbor pairs were present (ordered). Table 3 shows the predicted Al ordering effects through the lens of Al concentration of the interfaces relative to the bulk phases. Ordering decreases the cohesive energy of the FCC matrix as well as the stacking fault energy values for the FCC matrix. Further variability can be expected if segregation effects to the interface are taken into account.

The effects of ordering and a distribution of possible interface energies can have a significant effect on the nucleation of the precipitates in various orientations. Using the results that are given by our potential, we applied classical nucleation theory using two possible values of the energy difference between the FCC and the B2, reflecting ordering effects (L (low) with nucleation energies per atom of 0.16 eV/atom and H (high) with nucleation energies per atom of 0.2 eV/atom). We then considered three possible values of the interface energies that roughly span the range of interface energies predicted by our molecular dynamics simulations (L, M, H corresponding to 0.8 J/m<sup>2</sup>, 0.96 J/m<sup>2</sup>, and

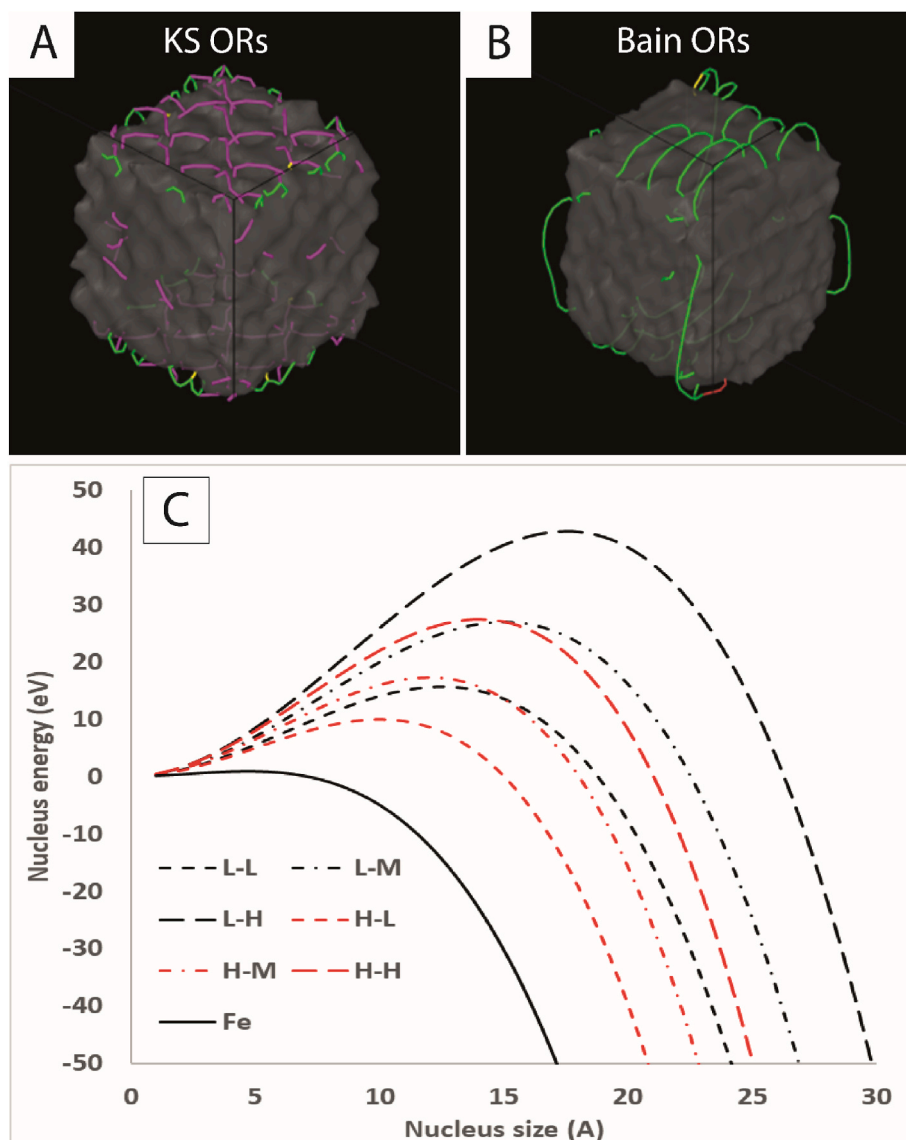


**Fig. 4.** Misfit dislocation arrays observed for precipitates in the A) KS, and B) Bain orientation relationships. Nucleation barriers given by classical nucleation theory assuming three different values of the interface energy and two different values of the energy difference between the two phases(C). The estimates are consistent with values given by the potentials utilized in the simulations.

1.12 J/m<sup>2</sup>). Fig. 4C shows energy evolution as the nucleus grows in all six combinations. For comparison with a simpler non-ordering system, reasonable estimates for the nucleation of the BCC phase in pure FCC Fe are also included, using an energy difference between the FCC and BCC phases of 0.15 eV and an interface energy of 0.22 J/m<sup>2</sup> [79].

Critical nucleus sizes are given by the maxima in the curves shown in Fig. 4C and are around 1.3 nm–1.6 nm, or about 200 atoms to 500 atoms. It is important to emphasize the role of compositional complexity on interface energetics and nucleation behavior. In pure Fe, the FCC/BCC interface energies are significantly lower, and the critical nucleus size is approximately 0.5 nm (just a few atoms). In contrast, complex alloys exhibit interface energy variations influenced by the local distribution of constituent elements. Fluctuations in local chemical order, caused by the inherent complexity of the alloy, further broaden the range of possible interface energies. This variability, in turn, impacts the critical nucleus size and nucleation barriers in HEAs compared to pure metals. Our simulations using empirical potential indicate a wide range of possible interface energies in complex alloys. While the results are semiquantitative and the specific atomic-scale interface structures have yet to be experimentally verified, they provide insight into the potential

multiplicity and complexity of interface configurations. It is also clear from the estimates that changes in the ordering state of the FCC can also affect which orientation is nucleated. These complexities at the nucleation stage can contribute to the observation of various non-traditional orientation relationships in HEA alloys. Future work using high-resolution TEM (HRTEM) characterization of these interfaces in complex alloys can further confirm these predictions.

#### 4. Conclusion

The toolset described above was combined to investigate the impact of compositional and chemical order complexity on OR formation mechanisms. This work provides an initial view of how local fluctuations in structural and chemical order can influence preferred ORs. We combined EXELFS and EXAFS to study the local chemistry in Al<sub>0.3</sub>CoCrFeNi. Our results show that the average effective bond lengths of Cr–M, Ni–M, and Co–M bonds decrease after aging, and that Cr–M bonding becomes less favorable. TEM characterization revealed the formation of new ORs between the BCC and FCC phases, driven by local chemical complexity. Specifically, we report the presence of two B2

phases in the aged alloy, each exhibiting a distinct OR: one follows the typical KS OR, while the other shows an unusual relationship with the FCC matrix, where  $\langle 110 \rangle_{\text{FCC}}$  aligns with  $\langle 100 \rangle_{\text{BCC}}$ . These non-typical ORs can be attributed to the complex local chemistry observed in both the homogenized and aged states of the alloy, and to the associated energetic and structural fluctuations characteristic of HEAs.

The simulations demonstrate that compositional complexity and local ordering significantly impact interface structure, energy, and nucleation behavior. A wide range of interface energies ( $0.8\text{--}2\text{ J/m}^2$ ) was observed, with the lowest value associated with the KS OR and the highest with the non-typical OR. Interface thickness varied between 0.3 and 0.5 nm depending on the interface plane and OR. Local atomic relaxations led to variations in interface composition, particularly Al enrichment, and different degrees of atomic matching at the interface. Dislocation structures also varied with orientation, with some ORs showing Shockley partials or stair-rod networks, while others remained dislocation-free. Nucleation analysis based on classical theory indicates that these variations translate into larger critical nucleus sizes in HEAs compared to pure metals. The results emphasize that local chemical and structural disorder in complex alloys directly affects interface energetics and can lead to non-traditional orientation relationships.

The combination of interatomic potentials and innovative, multiscale microscopy techniques provides a toolset to explore the consequences of chemical complexity in HEAs, particularly in the development of multiphase microstructures. The findings resulting from this work will provide a foundation to explore currently untapped compositional space toward alloy phase evolution.

#### CRediT authorship contribution statement

**Elaf A. Anber:** Writing – review & editing, Writing – original draft, Visualization, Validation, Methodology, Investigation, Formal analysis, Conceptualization. **Daniel L. Foley:** Writing – review & editing, Visualization, Investigation, Formal analysis. **James L. Hart:** Writing – review & editing, Formal analysis, Data curation, Investigation. **Howie Jorress:** Writing – review & editing, Visualization, Formal analysis, Investigation. **Brian DeCost:** Visualization, Validation, Formal analysis, Data curation. **Roger Doherty:** Writing – review & editing, Visualization. **Peter K. Liaw:** Writing – review & editing, Visualization. **Diana Farkas:** Writing – review & editing, Visualization, Validation, Methodology, Formal analysis, Data curation. **Anatoly I. Frenkel:** Writing – review & editing, Visualization, Validation, Supervision, Formal analysis, Data curation, Conceptualization. **Mitra L. Taheri:** Writing – review & editing, Visualization, Validation, Supervision, Methodology, Conceptualization.

#### Declaration of competing interest

The authors declare that they have no known competing financial interests or personal relationships that could have appeared to influence the work reported in this paper.

#### Acknowledgment

This research used resources at the 6-BM beamline of the National Synchrotron Light Source II, a U.S. Department of Energy (DOE) Office of Science User Facility operated for the DOE Office of Science by Brookhaven National Laboratory under Contract No. DE-SC0012704. The authors acknowledge funding, in part (E.A.A. J.L.H. and M.L.T.), from the National Science Foundation MRI program (Award No. 1429661) and, in part (M.L.T.), from the Office of Naval Research through the Multidisciplinary University Research Initiative (MURI) program (Award No. N00014-20-1-2368) with program manager David Shifler. A. I. F. acknowledges support from the National Science Foundation (Grant No. CHE 2203858) for his contribution to the EXELFS data analysis and interpretation. M.L.T. acknowledges support from the

United State Department of Defense ONR grant No. N00014-20-1-2788. P.K.L. acknowledges support from (1) the Army Office Projects (Grant Nos. W911NF-13-1-0438 and W911NF-19-2-0049) with program managers Michael P. Bakas, David M. Stepp, and S. Mathaudhu and (2) the National Science Foundation (Grant Nos. DMR-1611180 and 1809640) with program directors Judith Yang, Gary Shiflet, and Diana Farkas. The authors are grateful to Dr. Bruce Ravel (National Institute of Standards and Technology), for assistance and guidance for successful XAFS measurements. Certain equipment, instruments, software, or materials are identified in this paper to specify the experimental procedure adequately. Such identification is not intended to imply recommendation or endorsement of any product or service, nor is it intended to imply that the materials or equipment identified are necessarily the best available for the purpose.

#### Appendix A. Supplementary data

Supplementary data to this article can be found online at <https://doi.org/10.1016/j.intermet.2025.108832>.

#### Data availability

Data will be made available on request.

#### References

- [1] D.B. Miracle, O.N. Senkov, A critical review of high entropy alloys and related concepts, *Acta Mater.* 122 (2017) 558, <https://doi.org/10.1016/j.actamat.2016.12.024>, 511.
- [2] B.J. Yeh, S. Chen, S. Lin, J. Gan, T. Chin, T. Shun, C. Tsau, Nanostructured high-entropy alloys with multiple principal elements: novel alloy design concepts and outcomes, *Acta Mater.* 52 (2004) 299–303, <https://doi.org/10.1002/adem.200300567>.
- [3] B. Cantor, I.T.H. Chang, P. Knight, A.J.B. Vincent, Microstructural development in equiatomic multicomponent alloys, *Mater. Sci. Eng. A* 375–377 (2004) 213–218, <https://doi.org/10.1016/j.msea.2003.10.257>.
- [4] Y. Zhang, T.T. Zuo, Z. Tang, M.C. Gao, K.A. Dahmen, P.K. Liaw, Z.P. Lu, Microstructures and properties of high-entropy alloys, *Prog. Mater. Sci.* 61 (2014) 1–93, <https://doi.org/10.1016/j.pmatsci.2013.10.001>.
- [5] O.N. Senkov, G.B. Wilks, J.M. Scott, D.B. Miracle, Mechanical properties of Nb<sub>25</sub>Mo<sub>25</sub>Ta<sub>25</sub>W<sub>25</sub> and V<sub>20</sub>Nb<sub>20</sub>Mo<sub>20</sub>Ta<sub>20</sub>W<sub>20</sub> high entropy alloys, *Intermetallics* 19 (2011) 697–706, <https://doi.org/10.1016/j.intermet.2011.01.004>.
- [6] F. Otto, A. Dlouhy, H. Bei, O. Ridge, G. Eggeler, The influences of temperature and microstructure on the tensile properties of a CoCrFeMnNi high-entropy alloy, *Acta Mater.* 61 (2013) 382–392, <https://doi.org/10.1016/j.actamat.2013.06.018>.
- [7] B. Gwalani, S. Gorsse, D. Choudhuri, M. Styles, Y. Zheng, R.S. Mishra, R. Banerjee, Modifying transformation pathways in high entropy alloys or complex concentrated alloys via thermo-mechanical processing, *Acta Mater.* 153 (2018) 169–185, <https://doi.org/10.1016/j.actamat.2018.04.021>.
- [8] X.G. Li, C. Chen, H. Zheng, Y. Zuo, S.P. Ong, Complex strengthening mechanisms in the NbMoTaW multi-principal element alloy, *npj Comput. Mater.* 6 (2020) 1–10, <https://doi.org/10.1038/s41524-020-0311-4>.
- [9] Y.J. Liang, L. Wang, Y. Wen, B. Cheng, Q. Wu, T. Cao, Q. Xiao, Y. Xue, G. Sha, Y. Wang, Y. Ren, High-content ductile coherent nanoprecipitates achieve ultrastrong high-entropy alloys, *Nat. Commun.* 9 (2018) 1–8, <https://doi.org/10.1038/s41467-018-05372-1>.
- [10] V. Soni, O.N. Senkov, B. Gwalani, D.B. Miracle, R. Banerjee, Microstructural design for improving ductility of an initially brittle refractory high entropy alloy, *Sci. Rep.* 8 (2018) 1–10, <https://doi.org/10.1038/s41598-018-21031-8>.
- [11] O.N. Senkov, D. Isheim, D.N. Seidman, A.L. Pilchak, Development of a refractory high entropy superalloy, *Entropy* 18 (2016) 102, <https://doi.org/10.3390/e18030102>.
- [12] G. Laplanche, J. Bonneville, C. Varvenne, W.A. Curtin, E.P. George, Thermal activation parameters of plastic flow reveal deformation mechanisms in the CrMnFeCoNi high-entropy alloy, *Acta Mater.* 143 (2018) 257–264, <https://doi.org/10.1016/j.actamat.2017.10.065>.
- [13] C. Varvenne, G.P.M. Leyson, M. Ghazisaeidi, W.A. Curtin, Solute strengthening in random alloys, *Acta Mater.* 124 (2017) 660–683, <https://doi.org/10.1016/j.actamat.2016.11.049>.
- [14] C. Varvenne, A. Luque, W.A. Curtin, Theory of strengthening in fcc high entropy alloys, *Acta Mater.* 118 (2016) 164–176, <https://doi.org/10.1016/j.actamat.2016.07.036>.
- [15] C. Varvenne, W.A. Curtin, Predicting yield strengths of noble metal high entropy alloys, *Scr. Mater.* 142 (2018) 92–95, <https://doi.org/10.1016/j.scriptamat.2017.10.033>.
- [16] D.S. Wen, M.S. Titus, SSpredict: A Solid Solution Strengthening Prediction and Visualization Tool, 2019, <https://doi.org/10.5281/zenodo.2631415>.

- [17] T.M. Smith, M.S. Hooshmand, B.D. Esser, F. Otto, D.W. McComb, E.P. George, M. Ghazisaeidi, M.J. Mills, Atomic-scale characterization and modeling of dislocations in a high-entropy alloy, *Acta Mater.* 110 (2016) 352–363, <https://doi.org/10.1016/j.actamat.2016.03.045>.
- [18] R.S. Mishra, N. Kumar, M. Komarasamy, Lattice strain framework for plastic deformation in complex concentrated alloys including high entropy alloys, *Mater. Sci. Technol.* 31 (2015) 1259–1263, <https://doi.org/10.1179/1743284715Y.0000000050>.
- [19] M. Komarasamy, N. Kumar, R.S. Mishra, P.K. Liaw, Anomalies in the deformation mechanism and kinetics of coarse-grained high entropy alloy, *Mater. Sci. Eng. A* 654 (2016) 256–263, <https://doi.org/10.1016/j.msea.2015.12.063>.
- [20] C. Lee, G. Song, M.C. Gao, R. Feng, P. Chen, J. Brechtel, Y. Chen, K. An, W. Guo, J. D. Poplawsky, S. Li, Lattice distortion in a strong and ductile refractory high-entropy alloy, *Acta Mater.* 160 (2018) 158–172, <https://doi.org/10.1016/j.actamat.2018.08.013>.
- [21] Y. Ma, Q. Wang, B.B. Jiang, C.L. Li, J.M. Hao, X.N. Li, C. Dong, T.G. Nieh, Controlled formation of coherent cuboidal nanoprecipitates in body-centered cubic high-entropy alloys based on Al<sub>2</sub>(Ni, Co, Fe, Cr)<sub>14</sub> compositions, *Acta Mater.* 147 (2018) 213–225, <https://doi.org/10.1016/j.actamat.2018.01.056>.
- [22] S. Huang, W. Li, E. Holmström, L. Vitos, Strengthening induced by MagnetoChemical transition in Al-doped Fe-Cr-Co-Ni high-entropy alloys, *Phys. Rev. Appl.* 10 (2018) 064033, <https://doi.org/10.1103/PhysRevApplied.10.064033>.
- [23] W.-Z. Zhang, G.C. Weatherly, On the crystallography of precipitation, *Prog. Mater. Sci.* 50 (2005) 181–292, <https://doi.org/10.1016/j.pmatsci.2004.04.002>.
- [24] U. Dahmen, Orientation relationships in precipitation systems, *Acta* 30 (1982) 63–73, [https://doi.org/10.1016/0001-6160\(82\)90092-6](https://doi.org/10.1016/0001-6160(82)90092-6).
- [25] D.A. Porter, K.E. Easterling, *Phase Transformations in Metals and Alloys*, third ed., CRC Press, 1992.
- [26] M. Nastar, L.T. Belkacemi, E. Meslin, Thermodynamic model for lattice point defect-mediated semi-coherent precipitation in alloys, *Commun Mater* 2 (2021) 32, <https://doi.org/10.1038/s43246-021-00136-z>.
- [27] Y. Matsukawa, Crystallography of precipitates in metals and alloys: (1) analysis of crystallography, in: T. Akitasu (Ed.), *Crystallography*, IntechOpen, 2019, <https://doi.org/10.5772/intechopen.82693>.
- [28] D. Choudhuri, et al., Crystallographically degenerate B2 precipitation in a plastically deformed FCC-based complex concentrated alloy, *Mater. Res. Lett.* 6 (2018) 171–177, <https://doi.org/10.1080/21663831.2018.1443684>.
- [29] Y. He, J. Gao, Y. He, K. Shin, A new FCC-BCC orientation relationship observed in the strain-induced martensitic transformation of an austenitic stainless steel, *Mater. Lett.* 305 (2021) 130735, <https://doi.org/10.1016/j.matlet.2021.130735>.
- [30] T.J. Headley, J.A. Brooks, A new BCC-FCC orientation relationship observed between ferrite and austenite in solidification structures of steels, *Metall. Mater. Trans. A* 33 (2002) 5–15, <https://doi.org/10.1007/s11661-002-0001-0>.
- [31] D. Choudhuri, S. Shukla, W.B. Green, B. Gwalani, V. Ageh, R. Banerjee, R. S. Mishra, Crystallographically degenerate B2 precipitation in a plastically deformed FCC-based complex concentrated alloy, *Mater. Res. Lett.* 6 (2018) 171–177, <https://doi.org/10.1080/21663831.2018.1443684>.
- [32] J.C. Rao, V. Ocelik, D. Vainchtein, Z. Tang, P.K. Liaw, J.T.M. De Hosson, The FCC-BCC crystallographic orientation relationship in Al<sub>x</sub>CoCrFeNi high-entropy alloys, *Mater. Lett.* 176 (2016) 29–32, <https://doi.org/10.1016/j.matlet.2016.04.140>.
- [33] F.X. Zhang, S. Zhao, K. Jin, H. Xue, G. Velisa, H. Bei, R. Huang, J.Y.P. Ko, D. C. Pagan, J.C. Neufeld, W.J. Weber, Local structure and short-range order in a NiCoCr solid solution alloy, *Phys. Rev. Lett.* 118 (20) (2017) 1–6, <https://doi.org/10.1103/PhysRevLett.118.205502>.
- [34] J.G. Goini, S.K. Kolli, A. Van Der Ven, Role of short- and long-range ordering on diffusion in Ni-Al alloys, *Phys. Rev. Mater.* 3 (9) (2019) 1–12, <https://doi.org/10.1103/PhysRevMaterials.3.093603>.
- [35] R.C. Newman, A percolation model for passivation in stainless steels, *J. Electrochem. Soc.* 133 (9) (1986) 1979–1980, <https://doi.org/10.1149/1.2108617>.
- [36] S. Qian, R.C. Newman, R.A. Cottis, K. Sieradzki, Validation of a percolation model for passivation of Fe-Cr alloys: two-dimensional computer simulations, *J. Electrochem. Soc.* 137 (2) (1990) 435–439, <https://doi.org/10.1149/1.2086926>.
- [37] S. Qian, R.C. Newman, R.A. Cottis, K. Sieradzki, Computer simulation of alloy passivation and activation, *Corros. Sci.* 31 (C) (1990) 621–626, [https://doi.org/10.1016/0010-938X\(90\)90087-4](https://doi.org/10.1016/0010-938X(90)90087-4).
- [38] M.-H. Tsai, J.-W. Yeh, High-entropy alloys: a critical review, *Mater. Res. Lett.* 2 (3) (2014) 107–123, <https://doi.org/10.1080/21663831.2014.927366>.
- [39] V.K.S. Shante, S. Kirkpatrick, An introduction to percolation theory, *Adv. Phys.* (1971) 1–122, <https://doi.org/10.1080/00018737100101261>.
- [40] M. Liu, A. Aiello, Y. Xie, K. Sieradzki, The effect of short-range order on passivation of Fe-Cr alloys, *Metall. Mater. Trans. A* 49 (11) (2018) 830–834, <https://doi.org/10.1007/s11661-018-4606-9>.
- [41] Q. Li, H. Sheng, E. Ma, Pathways, *Nat. Commun.* (2019) 1–11, <https://doi.org/10.1038/s41467-019-08601-2>.
- [42] Daniel L. Foley, Annie K. Barnett, Yevgeny Rakita, Alejandro Perez, Partha Pratim Das, Stavros Nicolopoulos, Douglas E. Spearot, Irene J. Beyerlein, Michael L. Falk, Mitra L. Taheri, Diffuse electron scattering reveals kinetic frustration as origin of order in CoCrNi medium entropy alloy, *Acta Mater.* 268 (2024) 119753, <https://doi.org/10.1016/j.actamat.2024.119753>.
- [43] S. Maiti, W. Steurer, Structural disorder and its effect on the mechanical properties in single-phase TaNbHfZr high-entropy alloys, *Acta Mater.* 106 (2016) 87–97, <https://doi.org/10.1016/j.actamat.2016.01.018>.
- [44] D.L. Foley, T. Radetic, M.L. Taheri, Evolution of  $\beta$ -phase precipitates in an aluminum-magnesium alloy at the nanoscale, *Acta Mater.* 185 (2020) 279–286, <https://doi.org/10.1016/j.actamat.2019>.
- [45] J. Nie, Precipitation and hardening in magnesium alloys, *Mater. Sci. Eng. A* 43 (November) (2012), <https://doi.org/10.1016/j.msea.2012.05.057>.
- [46] D. Farkas, A. Caro, Model interatomic potentials for Fe-Ni-Cr-Co-Al high-entropy alloys, *J. Mater. Res.* 35 (22) (2020) 3031–3040, <https://doi.org/10.1557/jmr.2020.359>.
- [47] Necip Ünlü, Preparation of high-quality Al TEM specimens via a double-jet electropolishing technique, *Mater. Charact.* 59 (5) (2008) 547–553, <https://doi.org/10.1016/j.matchar.2007.04.003>.
- [48] E.A. Anber, A.C. Lang, E.A. Lass, P.K. Suri, J.L. Hart, D.S. D'Antuono, et al., Insight into the kinetic stabilization of Al<sub>0.3</sub>CoCrFeNi high-entropy alloys, *Materialia* 14 (2020) 100872, <https://doi.org/10.1016/j.mta.2020.100872>.
- [49] Elaf A. Anber, Nathan C. Smith, Peter K. Liaw, Christopher M. Wolverton, Mitra L. Taheri, Role of Al additions in secondary phase formation in CoCrFeNi high entropy alloys, *APL Mater.* 10 (2022) 000000, <https://doi.org/10.1063/5.0117280>.
- [50] Elaf A. Anber, Andrew C. Lang, Eric A. Lass, Pranav Kumar Suri, Daniel Scott D'Antuono, Haoyan Diao, Peter K. Liaw, Mitra L. Taheri, Early stages of secondary phase formation in multicomponent alloys using an in-situ TEM heating approach, *Microsc. Microanal.* 25 (S2) (2019) 1536–1537, <https://doi.org/10.1017/S1431927619008541>.
- [51] Elaf A. Anber, Andrew C. Lang, Eric A. Lass, Pranav Kumar Suri, Daniel Scott D'Antuono, Haoyan Diao, Peter K. Liaw, Mitra L. Taheri, Thermal stability of high entropy alloys during in situ TEM heating, *Microsc. Microanal.* 24 (S1) (2018) 1928–1929, <https://doi.org/10.1017/S1431927618014052>.
- [52] J.L. Hart, A.C. Lang, A.C. Leff, P. Longo, C. Trevor, R.D. Twisten, M.L. Taheri, Direct detection electron energy-loss spectroscopy: a method to push the limits of resolution and sensitivity, *Sci. Rep.* (2017) 1–14, <https://doi.org/10.1038/s41598-017-07709-4>.
- [53] James L. Hart, Kanit Hantanasirisakul, Andrew C. Lang, Yuanyuan Li, Faisal Mehmood, Ruth Pachter, Anatoly I. Frenkel, Yury Gogotsi, Mitra L. Taheri, Multimodal spectroscopic study of surface termination evolution in Cr<sub>2</sub>TiC<sub>2</sub>X MXene, *Adv. Mater. Interfaces* 8 (2021) 2001789, <https://doi.org/10.1002/admi.202001789>.
- [54] J.L. Hart, A.C. Lang, Y. Li, S. Shahrezaei, D.D. Alix-Williams, M.L. Falk, S. N. Mathaudhu, A.I. Frenkel, M.L. Taheri, Revealing local order via high energy EELS, *Mater. Today Nano* 21 (2023) 100298, <https://doi.org/10.1016/j.mtnano.2022.100298>.
- [55] A.I. Frenkel, Q. Wang, S.I. Sanchez, M.W. Small, R.G. Nuzzo, Short range order in bimetallic nanoalloys: an extended X-ray absorption fine structure study, *J. Phys. Chem. C* 114 (2010) 14211–14218, <https://doi.org/10.1021/jp104530m>.
- [56] A. Frenkel, E.A. Stern, A. Voronel, M. Qian, M. Newville, Solving the structure of disordered mixed salts, *Phys. Rev. B* 49 (1994) 11662, <https://doi.org/10.1103/PhysRevB.49.11662>.
- [57] A. Frenkel, E.A. Stern, A. Voronel, M. Qian, M. Newville, Buckled crystalline structure of mixed ionic salts, *Phys. Rev. Lett.* 71 (1993) 3485, <https://doi.org/10.1103/PhysRevLett.71.3485>.
- [58] A. Frenkel, E.A. Stern, A. Voronel, S. Heald, Lattice strains in disordered mixed salts, *Solid State Commun.* 99 (1996) 67, [https://doi.org/10.1016/S0038-1098\(96\)00335-1](https://doi.org/10.1016/S0038-1098(96)00335-1).
- [59] A.I. Frenkel, V. Sh Machavariani, A. Rubshten, Yu Rosenberg, A. Voronel, E. A. Stern, Local structure of disordered Au-Cu and Au-Ag alloys, *Phys. Rev. B* 62 (2000) 9364–9371, <https://doi.org/10.1103/PhysRevB.62.9364>.
- [60] A.I. Frenkel, Applications of extended X-ray absorption fine structure spectroscopy to studies of bimetallic nanoparticle catalysts, *Chem. Soc. Rev.* 41 (2012) 8163–8178, <https://doi.org/10.1039/C2CS35124E>.
- [61] A.C. Foucher, S. Yang, D.J. Rosen, R. Huang, J.B. Pyo, O. Kwon, C.J. Owen, D. F. Sanchez, I.I. Sadykov, D. Grolimund, B. Kozinsky, A.I. Frenkel, R.J. Gorte, C. B. Murray, E.A. Stach, Synthesis and characterization of stable Cu–Pt nanoparticles under reductive and oxidative conditions, *J. Am. Chem. Soc.* 145 (9) (2023) 5410–5421, <https://doi.org/10.1021/jacs.3c00955>.
- [62] A.C. Foucher, N. Marcella, J.D. Lee, R. Tappero, C.B. Murray, A.I. Frenkel, E. A. Stach, Dynamical change of valence states and structure in NiCu<sub>3</sub> nanoparticles during redox cycling, *J. Phys. Chem. C* 126 (4) (2022) 1991–2002, <https://doi.org/10.1021/acs.jpcc.1c10780>.
- [63] D. Farkas, A. Caro, *J. Mater. Res.* 33 (19) (2018) 3218–3225, <https://doi.org/10.1557/jmr.2018.234>.
- [64] S. Plimpton, Fast parallel algorithms for short-range molecular-dynamics, *J. Comput. Phys.* 117 (1) (1995) 1–19, <https://doi.org/10.1006/jcph.1995.1036>.
- [65] A. Stukowski, Visualization and analysis of atomistic simulation data with OVITO—the Open Visualization Tool, *Modell. Simul. Mater. Sci. Eng.* 18 (1) (2010), <https://doi.org/10.1088/0965-0393/18/1/015012>.
- [66] Wei Fang, Haoyang Yu, Ruobin Chang, Xin Zhang, Puguang Ji, Baoxi Liu, Li Jia, Xuanhui Qu, Ye Liu, Fuxing Yin, Microstructure and mechanical properties of Cr-rich Co-Cr-Fe-Ni high entropy alloys designed by valence electron concentration, *Mater. Chem. Phys.* 238 (2019) 121897, <https://doi.org/10.1016/j.matchemphys.2019.121897>.
- [67] L.D. Menard, Q. Wang, J.H. Kang, A. Sealey, G.S. Girolami, X. Teng, A.I. Frenkel, R. G. Nuzzo, Structural characterization of bimetallic nanomaterials with overlapping x-ray absorption edges, *Phys. Rev. B* 80 (2009) 064111, <https://doi.org/10.1103/PhysRevB.80.064111>.
- [68] W.-R. Jian, X. Zhang, H. Wang, W. Zhang, Z. Chen, P.K. Liaw, Effects of lattice distortion and chemical short-range order on the mechanisms of deformation in

- medium entropy alloy CoCrNi, *Acta Mater.* 199 (2020) 352–369, <https://doi.org/10.1016/j.actamat.2020.08.051>.
- [69] D.L. Foley, H. Li, M.L. Taheri, D.C. Dunand, Simultaneous twinning and microband formation under dynamic compression in a high entropy alloy with a complex energetic landscape, *Acta Mater.* 200 (2020) 1–11, <https://doi.org/10.1016/j.actamat.2020.11.004>.
- [70] S. Bajpai, R. Kaur, A. Kumar, A. Mukhopadhyay, Recent progress in the CoCrNi alloy system, *Materialia* 24 (2022) 101476, <https://doi.org/10.1016/j.mtla.2022.101476>.
- [71] T.M. Smith, M.S. Hooshmand, B.D. Esser, C. Niu, M.J. Mills, M. Ghazisaeidi, Atomic-scale characterization and modeling of 60° dislocations in a high-entropy alloy, *Acta Mater.* 110 (2016) 352–363, <https://doi.org/10.1016/j.actamat.2016.03.045>.
- [72] A. Gupta, W.-R. Jian, S. Xu, I.J. Beyerlein, G.J. Tucker, On the deformation behavior of CoCrNi medium entropy alloys: unraveling mechanistic competition, *Int. J. Plast.* 159 (2022) 103442, <https://doi.org/10.1016/j.ijplas.2022.103442>.
- [73] J. Ding, Q. Yu, M. Asta, R.O. Ritchie, Tunable stacking fault energies by tailoring local chemical order in CrCoNi medium-entropy alloys, *Proc. Natl. Acad. Sci.* 115 (36) (2018) 8919–8924, <https://doi.org/10.1073/pnas.1809723115>.
- [74] L.T.H. De Jeer, V. Ocelík, J.T.M. De Hosson, Orientation relationships in Al<sub>0.7</sub>CoCrFeNi high-entropy alloy, *Microsc. Microanal.* 23 (2017) 905–915, <https://doi.org/10.1017/S1431927617012442>.
- [75] R.S. Mishra, N. Kumar, M. Komarasamy, Lattice strain framework for plastic deformation in complex concentrated alloys including high entropy alloys, *Mater. Sci. Technol.* 31 (2015), <https://doi.org/10.1179/1743284715Y.0000000050>.
- [76] S. Zhao, Y.N. Osetsky, Y. Zhang, Atomistic insight into the effects of order, disorder and their interface on defect evolution, *J. Alloys Compd.* 859 (2021) 157770, <https://doi.org/10.1016/j.jallcom.2020.157770>.
- [77] L. Feng, Y. Xia, V. Soni, Y. Liu, Y. Zhang, Localized phase transformation at stacking faults and mechanism-based alloy design, *Acta Mater.* 240 (2022) 118287, <https://doi.org/10.1016/j.actamat.2022.118287>.
- [78] F. Kies, M. Yang, S. Neumeier, G. Laplanche, Enhanced precipitation strengthening of multi-principal element alloys by  $\kappa$ - and B2-phases, *Mater. Des.* 198 (2021) 109315, <https://doi.org/10.1016/j.matdes.2020.109315>.
- [79] J.K. Chen, D. Farkas, W.T. Reynolds, Atomistic simulation of an f.c.c./b.c.c. interface in Ni-Cr alloys, *Acta Mater.* 45 (11) (1997) 4415–4421, [https://doi.org/10.1016/S1359-6454\(97\)00048-4](https://doi.org/10.1016/S1359-6454(97)00048-4).